Available online at www.sciencedirect.com
ScienceDirect
Surface & Coatings Technology 201 (2007) 7692–7698
SURFACE & COATINGS TECHNOLOGY
www.elsevier.com/locate/surfcoat

# Phase segregation and its effect on the adhesion of Cr–Al–N coatings on K38G alloy prepared by magnetron sputtering method

Tianpeng Li [a,b], Meishuan Li [a], Yanchun Zhou [a,*]

[a] *High Performance Ceramic Division, Shenyang National Laboratory for Materials Science, Institute of Metal Research, Chinese Academy of Sciences, 72 Wenhua Road, Shenyang, 110016, China*
[b] *Graduate School of Chinese Academy of Sciences, Beijing, 100039, China*

Received 26 December 2006; accepted in revised form 27 February 2007
Available online 12 March 2007

**Abstract**

$Cr_{1-x}Al_xN$ ($0<x<1$) coatings were fabricated by a reactive magnetron sputtering method on a K38G alloy. The composition and microstructure of the coatings were investigated. Phase segregation of cubic AlN was considered in $Cr_{0.65}Al_{0.35}N$ using X-ray diffraction analyses. This segregation of cubic AlN from CrAlN matrix might be induced by the high micro-stress. The critical failure load determined by scratch tests of the coating with c-AlN segregation was highest among all the coatings studied in the present work, which indicated that the coating has the best adhesion.


*Keywords:* $Cr_{1-x}Al_xN$ coatings; Cubic AlN segregation; Residual stress; Scratch test

## 1. Introduction

It has been reported that the addition of aluminum is effective to improve the wear, corrosion and oxidation resistance of transition metal nitride coatings, such as TiN and CrN [1–7]. A number of previous works [8–11] reported the phase transition of Cr–Al–N coatings from B1 to B4 type structure when the AlN content exceeded 60–77 mol%. Cubic AlN was identified in TiN/AlN and VN/AlN multilayers or superlattices, which contributed to the significant improvement in mechanical properties of the multilayers or superlattice [12–14]. The metastable c-AlN is a high-pressure phase [15–18]. Setoyama et al. [19] predicted that c-AlN should have higher hardness and strength than h-AlN due to its higher volume density (~18%) compared with that of h-AlN. If c-AlN separates from CrAlN coatings, enhanced mechanical properties of the CrAlN coatings may be achieved. Phase segregation in CrAlN coatings is of both scientific interest and technological applications. However, few reports are available on the B1 phase segregation, i.e., B1 type Cr–Al–N coatings separated into CrN and c-AlN. On the other hand, the adhesion of coatings is one of the most important mechanical properties for industrial applications. The adhesion of Cr–Al–N coatings with different AlN contents has been investigated through scratch tests [20–22], but the effect of c-AlN segregation on the adhesion has not been reported.

In this work, the $Cr_{1-x}Al_xN$ ($0<x<1$) coatings were deposited and the phase segregation was found in a $Cr_{0.65}Al_{0.35}N$ coating. A phase segregation mechanism is proposed. Moreover, the effects of the c-AlN segregation on the adhesion of Cr–Al–N coatings are discussed based on scratch tests.

## 2. Experimental procedure

A K38G superalloy was chosen as the substrate in the present work. The nominal composition of the alloy is listed in Table 1. The alloy specimens were cut into dimensions of $25\times10\times2$ mm$^3$ by an electric-discharge method and their surfaces were ground down to 1200 grit SiC paper and then polished with 1.0 μm diamond paste. Afterwards, the samples were degreased ultrasonically in acetone, cleaned by distilled water and then dried.

* Corresponding author. Tel.: +86 24 23971765; fax: +86 24 23891320.
*E-mail address:* yczhou@imr.ac.cn (Y. Zhou).

0257-8972/$ - see front matter © 2007 Elsevier B.V. All rights reserved.
doi:10.1016/j.surfcoat.2007.02.044

Table 1
Nominal composition of K38G alloy

| Element | C | Cr | Co | W | Mo | Al | Ti | Fe | Nb | Ta | Zr | Ni |
|---|---|---|---|---|---|---|---|---|---|---|---|---|
| Content (%) | 0.13–0.20 | 15.3–16.8 | 8.0–9.0 | 2.3–2.9 | 1.4–2.0 | 3.5–4.5 | 3.20–4.00 | <0.20 | 0.40–1.00 | 1.4–2.0 | 0.05–0.15 | Bare |

Cr–Al–N coatings were prepared using a JGP560C14 magnetron sputtering system (SKY Technology Development Co. Ltd, Shenyang, China) by reactive magnetron co-sputtering from two targets of chromium (purity 99.99%) and aluminum (purity 99.99%) at 300 °C in a D.C mode. The substrates keep static during the deposition and the targets setup is shown schematically in Fig. 1. The deposition conditions are shown in Table 2. The AlN content in the CrAlN coatings was tuned by varying the power density of Cr and Al targets. For $Cr_{0.65}Al_{0.35}N$ coating, both the power density of Cr and Al targets are highest (7 W/cm$^2$) which results in the highest deposition rate. For the AlN content higher than 35 mol%, the power density of Cr target decreases and for the AlN content lower than 35 mol%, the power density of Al target decreases. The flow rates of the reactive gas ($N_2$, 99.999%) and the inert gas (Ar, 99.999%) were controlled by independent mass-flow controllers, and the gases were mixed before they entered the chamber. The thickness of the coatings was controlled to about 4 μm by adjusting the deposition time according to the deposition rate, which was determined based on the measurement of coatings thickness using scanning electron microscope (SEM).

After deposition, surface morphologies of the coatings were examined by a scanning electron microscope (SEM, LEO Super 35, Germany) and an atomic force microscope (AFM, CSPM-2000, China). The mean grain size and the root mean square roughness were calculated according to the images from AFM. X-ray diffraction (XRD, Rigaku D/max-2400, Japan) analyses were carried out to determine the phase component of the coatings. Lattice parameters and the full width at half maximum (FWHM) of the XRD peaks of the coatings were calculated using the Rietveld method [23]; which was accomplished in a DBWS program in the Cerius$^2$ software (Molecular simulation Inc., USA). The intensity of the XRD profile is represented by

$$I_{\text{Rietveld}}(2\theta) = b(2\theta) + s\sum_K L_K|F_K|^2\phi(2\theta_i - 2\theta_K)P_K A_K \qquad (1)$$

where $b(2\theta)$ is the background intensity, $s$ is a scale factor, $L_K$ contains the Lorentz, polarization and multiplicity factor, $\phi$ is the profile function, $P_K$ is the preferred orientation function, $A_K$ is the absorption factor and $F_K$ is the structure factor. The subscript $K$ represents Miller indices for the Bragg reflections.

In order to understand the effect of phase separation on the adhesion of coatings, scratch tests were conducted. Scratch test has been widely used in evaluating the coatings adhesion since it was first suggested for coatings adhesion measurements by Perry [24] and Valli [25]. It is a quick and empirical method to assess the critical load for coating failure. In this work, the scratch test was evaluated on a micro-tribometer system (CETR, USA) under ambient conditions (25 °C and 34% RH), wherein the progressive loading scratch test model was employed. A coated specimen was held rigidly in the sample holder and a Rockwell C diamond indenter with a tip radius of 0.2 mm was brought into contact with the coating surface. A normal load of 1 N was applied on the coating surface initially, and the load was kept constantly for 1 min. Then the normal load was increased linearly to 40 N in 1 min and the indenter was simultaneously moved at a speed of 10 mm/min. Friction coefficients were used to monitor the onset of coating failure. The scratch tracks were also observed by optical microscopy to determine the critical failure loads and the failure modes.

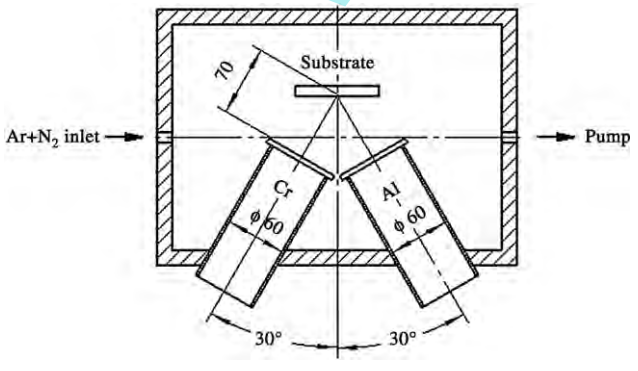


Fig. 1. Schematic drawing of the magnetron sputtering system setup in the vacuum chamber for the CrAlN coatings deposition.

## 3. Results

### 3.1. Effect of Al content on phase composition of Cr–Al–N coatings

Fig. 2(a) presents the XRD patterns of as-deposited $Cr_{1-x}Al_xN$ ($0<x<1$) coatings. Pseudobinary Cr–Al–N coatings are

Table 2
Deposition conditions of $Cr_{1-x}Al_xN$ ($0<x<1$) coatings

| Parameters | Value |
|---|---|
| Size of Cr and Al targets | Φ60 mm |
| Substrate size | 25 mm × 10 mm × 2 mm |
| Substrate temperature | 300 °C |
| Gas flow | Ar:$N_2$ = 12:8 (sccm) |
| Working pressure | 0.3 Pa |
| Base pressure | $2\times10^{-4}$ Pa |
| Power density of the targets | 1.7–7 W/cm$^2$ |
| Distance from each target to substrate | 70 mm |

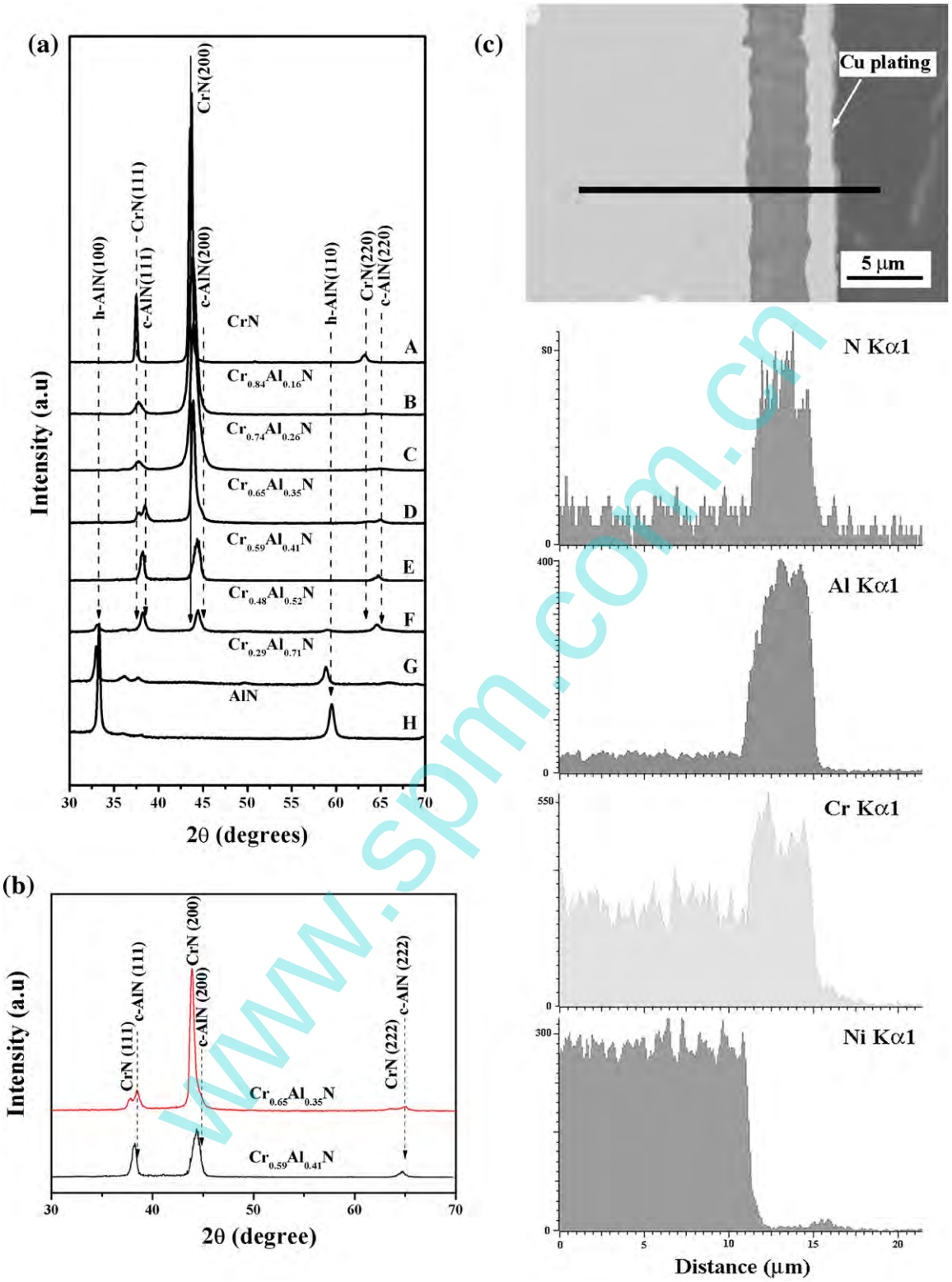


Fig. 2. The X-ray diffraction profiles for the as-deposited coatings prepared by magnetron sputtering on a K38G alloy, (a) for $Cr_{1-x}Al_xN$ ($0<x<1$), and (b) for the enlarged profile of $Cr_{0.65}Al_{0.35}N$ and $Cr_{0.59}Al_{0.41}N$ coatings, and the cross-section morphology together with the elements profile along the black line of the as-deposited $Cr_{0.65}Al_{0.35}N$ coating.

identified to be the B1 NaCl type crystal structure for CrN rich compositions (A, B, C, D and E in Fig. 2(a)), and to be the B4 wurtzite type crystal structure for AlN rich compositions (G and H in Fig. 2(a)). When the AlN content is in the range of 50–70 mol%, B1 and B4 type crystal structure coexist (F and G in Fig. 2(a)). The above results are in good agreement with

the theoretical prediction and the experimental result by Sugishima et al. [9]. Fig. 2(b) shows the enlarged XRD profile for $Cr_{0.65}Al_{0.35}N$ and $Cr_{0.59}Al_{0.41}N$ coatings. It is clearly seen that the (111) peak of $Cr_{0.65}Al_{0.35}N$ separated into two peaks and a shoulder can also be seen near the (200) peak on the right side, which indicates that phase segregation occurred. The newly appeared peaks correspond to the reflections of cubic aluminum nitride (JCPD card No. 46-1200), which is a high-pressure phase. As an example, Fig. 2(c) gives the cross-section together with the element profile along the black line of the as-deposited coating of $Cr_{0.65}Al_{0.35}N$, which indicates that the coating has homogenous compositions in the thickness. A fairly strong (200) preferred orientation is also seen when the AlN content is lower than 35 mol%. But the preferred orientation becomes weaker when the AlN content exceeds 35 mol%. In order to quantitatively compare the preferred orientation, the texture coefficients of (111) and (200) of the coatings with B1 type structure were calculated using the following equation [26]

$$T_{hkl} = \frac{I(hkl)\Big/I_0(hkl)}{\frac{1}{n}\left[\sum^{I(hkl)}\Big/I_0(hkl)\right]} \quad (2)$$

where $T_{hkl}$ is the texture coefficient of the ($hkl$) reflection, $n$ is the number of reflection planes being studied, $I(hkl)$ and $I_0(hkl)$ are the integrated intensities of ($hkl$) reflection for the coatings studied and that for the standard powder, respectively. The calculated texture coefficients are shown in Fig. 3. It is clearly seen that the (200) preferred orientation becomes weak when the AlN content is over 35 mol%.

The lattice parameters were calculated from the peak positions of (111) and (200) for B1 type structure and from (100) and (002) for B4 type structure. As shown in Fig. 4, with the increasing of AlN content the crystal structure of the coatings changes from B1 to B1+B4 and finally to B4. For $Cr_{0.65}Al_{0.35}N$, the lattice parameter was calculated according to the peaks of CrN. Linear fitting of the experimental data

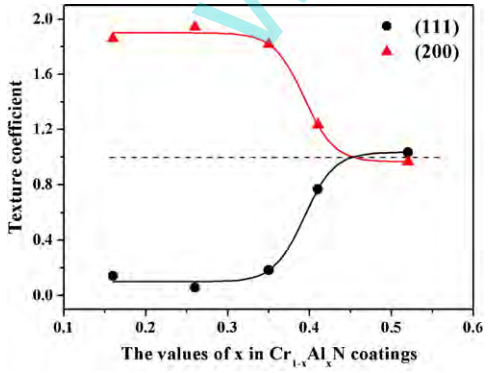


Fig. 3. Texture coefficients calculated by Eq. (2) for (111) and (200) reflection of $Cr_{1-x}Al_xN$ ($0.17<x<0.52$) coatings with B1 type crystal structure prepared by magnetron sputtering on a K38G alloy.

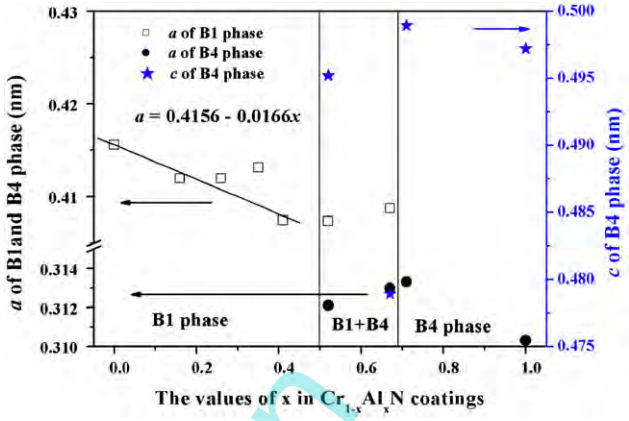


Fig. 4. Lattice parameters of the $Cr_{1-x}Al_xN$ ($0<x<1$) coatings calculated according to X-ray diffraction profiles by Rietveld method in the Cerius$^2$ computational program for material research.

indicates that the lattice parameter (in nanometer) of the B1 type structure can be described as:

$$a = 0.4156 - 0.0166x \quad (3)$$

where $x$ is AlN content in mol%. The lattice parameter of $Cr_{0.65}Al_{0.35}N$ has a deviation due to the segregation of c-AlN. When $x$ equals to 1, $a$ is 0.3990 nm, which is in good agreement with the lattice parameter of cubic AlN (0.4046 nm). Thus, it suggests that aluminum atoms in Cr–Al–N coatings with B1 type crystal structure are in the form similar to those in the high-pressure metastable phase, c-AlN [9].

### 3.2. Scratch test

Fig. 5(a) shows typical plot of the friction coefficient as a function of normal load in the scratch test. From the figure, three stages can be seen and two critical loads can be determined. An oscillation of the friction coefficient is found after the lower critical load, labeled as $L_{C1}$, is reached. The higher critical load, labeled as $L_{C2}$, is determined from a rapid increasing of the friction coefficient. The $L_{C1}$ denotes the initial failure of coatings, such as crackings and chippings, and $L_{C2}$ indicates the failure of coatings in the forms of spallation and breakthrough, as shown in Fig. 5(b) and (c). The critical load is linked to adhesion of coatings when spallation or breakthrough is observed. Therefore, $L_{C2}$ can be regarded as a sign for coatings adhesion failure, but $L_{C1}$ reflects the intrinsic mechanical properties of the coatings instead of coatings adhesion [27].

The changes of $L_{C1}$ and $L_{C2}$ for the coatings with different AlN contents are presented in Fig. 6. It is seen that $L_{C1}$ changes very slightly with the AlN content, which means that the intrinsic mechanical properties of the coatings change slightly with the AlN content increasing in the present work. However, $L_{C2}$ increases greatly with the AlN content and reaches a maximum value for $Cr_{0.65}Al_{0.35}N$, and then decreases with the further increasing of AlN content. The strongest adhesion of

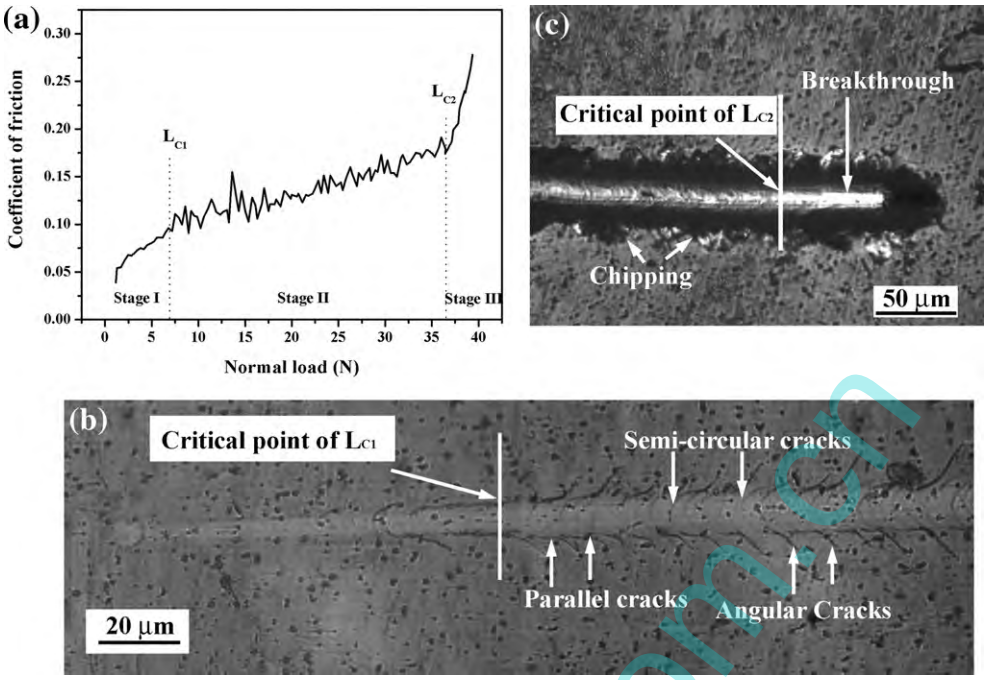


Fig. 5. (a) Typical plot of friction coefficient vs. normal load in the scratch tests of $Cr_{1-x}Al_xN$ ($0<x<0.52$) coatings, (b) and (c) are the corresponding optical micrographs for the scratch track when the normal load reaches $L_{C1}$ and $L_{C2}$, respectively.

the $Cr_{0.65}Al_{0.35}N$ coating may originate from the segregation of c-AlN from the CrAlN matrix (Fig. 2(a)–(b)).

## 4. Discussion

### 4.1. Formation mechanism of c-AlN

Cubic AlN is a high-pressure phase. At ambient temperature, it needs a pressure of more than 22 GPa for AlN to transform from hexagonal structure to the cubic structure [28–30]. Even at 1800 K, this transformation still needs a high pressure of 14–16.5 GPa [30]. In the present work, it never has such high pressure, but c-AlN presented in the $Cr_{0.65}Al_{0.35}N$ coating.

To understand the reason for the formation of c-AlN, FWHM of the XRD peaks for B1-CrAlN coatings was analyzed. As shown in Fig. 7, similar to the deposition rate, FWHM increases to a maximum and then decreases with the increasing AlN content. But as an exception, the FWHM of $Cr_{0.65}Al_{0.35}N$ is very low. The abnormal phenomena of low FWHM for $Cr_{0.65}Al_{0.35}N$ may be related to the formation of c-AlN.

Generally, the peak broadening of XRD profiles can be contributed to fine grain size and/or large residual micro-stress. Keeping other processing parameters constant, a higher deposition rate will result in a finer grain size and a higher micro-stress [31,32]. The deposition rate of $Cr_{0.65}Al_{0.35}N$ is the highest among all the coatings in the present work (Fig. 7). According to the results by Wuhrer and Yeung [31], the grain size decayed as an exponential relation with increasing deposition rate. Lugscheider et al. [32] indicated that the micro-stress will increase with the deposition rate increasing

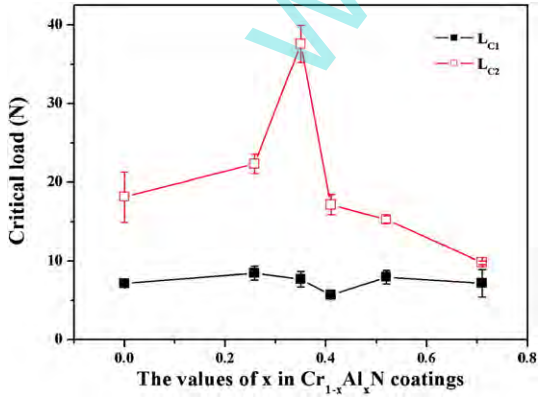


Fig. 6. Critical load $L_{C1}$ and $L_{C2}$ of $Cr_{1-x}Al_xN$ ($0<x<0.71$) coatings deposited on a K38G alloy as a function of Al contents, which were determined from scratch tests.

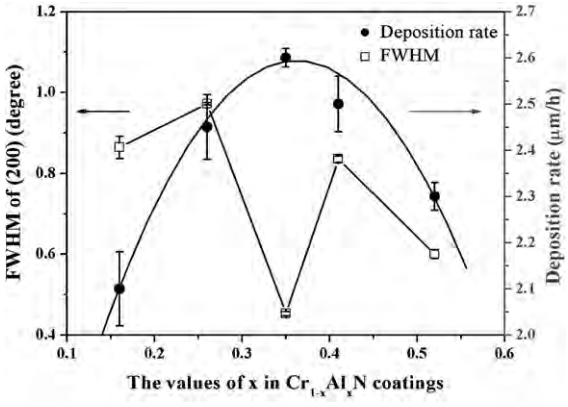


Fig. 7. FWHM together with the deposition rate of $Cr_{1-x}Al_xN$ ($0<x<0.52$) coatings deposited on a K38G alloy as a function of AlN content.

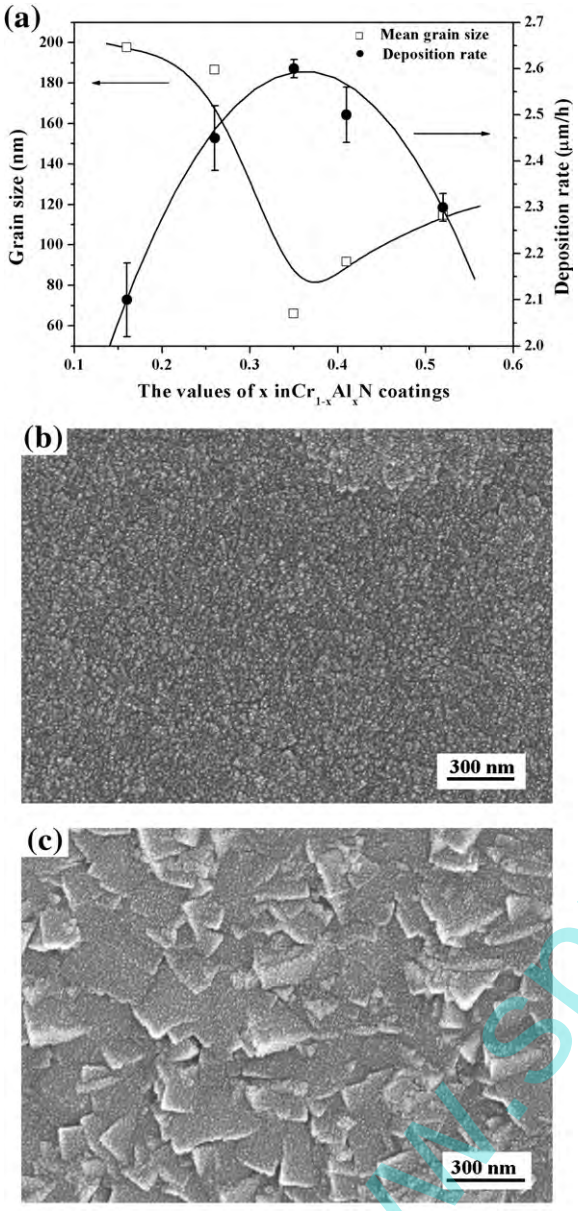


Fig. 8. (a) Grain size together with the deposition rate of $Cr_{1-x}Al_xN$ ($0.17<x<0.52$) coatings deposited on a K38G alloy as a function of AlN content and SEM images for the surface morphologies of (b) $Cr_{0.65}Al_{0.35}N$ and (c) $Cr_{0.84}Al_{0.16}N$.

because the crystal lattice of the coating is distorted due to the high kinetic energy of the incident ions. So the FWHM of $Cr_{0.65}Al_{0.35}N$ should be the largest because of both the finest grain size and the highest micro-stress. On the contrary, as shown in Fig. 7, FWHM of $Cr_{0.65}Al_{0.35}N$ is very low.

To clarify the mechanism of the low FWHM for the $Cr_{0.65}Al_{0.35}N$ coating, the mean grain size and lattice micro-strain were calculated. The mean grain size together with the deposition rate as a function of AlN content is shown in Fig. 8 (a). As expected, the $Cr_{0.65}Al_{0.35}N$ coating has a minimum grain size due to its high deposition rate. Fig. 8(b) and (c) give the typical SEM images for $Cr_{0.65}Al_{0.35}N$ and $Cr_{0.84}Al_{0.16}N$ coatings, respectively. It is clearly seen that the grain size of $Cr_{0.65}Al_{0.35}N$ is much smaller than that of $Cr_{0.84}Al_{0.16}N$.

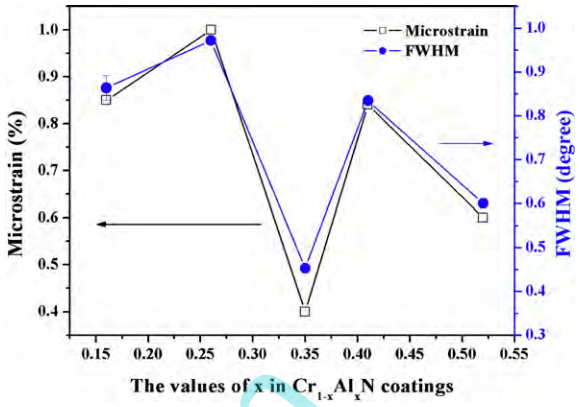


Fig. 9. Lattice microstrain calculated from Eq. (4) together with FWHM of $Cr_{1-x}Al_xN$ ($0<x<0.52$) coatings as a function of AlN content.

The lattice microstrain was calculated by the following equation [33]

$$\beta = \frac{0.9\lambda}{d\cos\theta} + \eta\tan\theta \tag{4}$$

where $\beta$ is FWHM of a XRD peak in degree, $\lambda$ is the wavelength of the radiation (in Å), $\theta$ is the Bragg angle, $d$ is the grain size (in Å), $\eta$ is the lattice microstrain.

The lattice microstrains together with the FWHM are shown in Fig. 9. It is surprising that the lattice microstrain of the $Cr_{0.65}Al_{0.35}N$ coating is the smallest despite of its highest deposition rate. Therefore, the most possible presumption for c-AlN formation is following. The high residual stress induces a phase separation, i.e., c-AlN segregates from Cr–Al–N matrix. This separation in turn contributes to the relaxation of the lattice microstrain. Consequently, the FWHM of the $Cr_{0.65}Al_{0.35}N$ coating became smaller. In addition, cubic TiN and VN in multilayers or superlattices were reported to contribute to the nucleation of c-AlN [15–17]. Thus, cubic CrN can also act as a template for the formation of c-AlN. The high-pressure phase formation induced by high stress was also reported for c-BN [34] and c-$Zr_3N_4$ [35], which supports our present results.

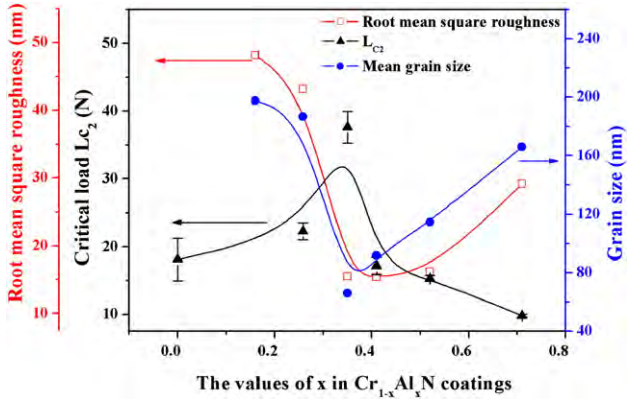


Fig. 10. Critical load $L_{C2}$ determined from scratch tests together with grain size and root mean square roughness (RMS) calculated from AFM images as a function of Al content of $Cr_{1-x}Al_xN$ ($0<x<1$) coatings.

### 4.2. Influence of phase segregation on the adhesion strength

Formation of c-AlN in the TiN/AlN and VN/AlN multilayers or superlattices resulted in improved mechanical properties [12–14]. Similarly, the $Cr_{0.65}Al_{0.35}N$ coating displayed a highest critical failure load due to the c-AlN segregation. The residual stresses in all the coatings are compressive because of the relatively lower thermal expansion coefficients compared with that of the K38G alloy substrate. An apropos compressive stress is beneficial for the adhesive strength of the coatings [36]. However, a large compressive stress will induce cracks, wrinkles, and even delamination, especially for ceramic coatings due to their intrinsic brittleness [37]. Therefore, if the compressive stress is high enough it will lead to a reduction of the adhesive strength. The separation of c-AlN significantly reduces the residual stress of the $Cr_{0.65}Al_{0.35}N$ coating. Accordingly, the high value of the critical failure loads for the $Cr_{0.65}Al_{0.35}N$ coating probably results from the apropos low residual compressive stress in the coating.

Fig. 10 depicts the mean grain size and the root mean square roughness together with the critical load $L_{C2}$ as a function of AlN content. It is clearly seen that $Cr_{0.65}Al_{0.35}N$ displays the smallest mean grain size and roughness. Thus, the high $L_{C2}$ of the $Cr_{0.65}Al_{0.35}N$ coating can also be attributed to the Hall-Petch effect and low concentration of the stress on the surface due to the small grain size and the small surface roughness.

## 5. Conclusion

Cr–Al–N coatings with different AlN contents have been prepared by a magnetron sputtering method. The type of the crystal structure of the coatings is related to AlN content. With increasing the AlN content to 50% and then to 70%, the crystal structure of the coatings change from B1 type to B1+B4, and then to B4, correspondingly. Phase segregation of the $Cr_{0.65}Al_{0.35}N$ coating into CrN and c-AlN has been considered. The mechanism has proposed, i.e., the phase segregation is induced by the high residual stress due to the high deposition rate. The critical failure load, $L_{C2}$, of the coatings increases with the AlN content and reaches a maximum value for $Cr_{0.65}Al_{0.35}N$, and then it decreases with further increasing AlN content. The highest value of $L_{C2}$ for $Cr_{0.65}Al_{0.35}N$ coating originates from c-AlN segregation from CrAlN matrix. The finer grain size and lower surface roughness also contribute to the high $L_{C2}$ of the $Cr_{0.65}Al_{0.35}N$ coating.

## Acknowledgements

This work was supported by the National Outstanding Young Scientist Foundation of China under grant No. 59925208, Natural Sciences Foundation of China under grant Nos. 50232040, 50571106, 50072034, 90403027, 863 project, and High-tech Bureau of the Chinese Academy of Sciences.

## References

[1] T. Ikeda, H. Satoh, Thin Solid Films 195 (1991) 99.
[2] Y. Makino, K. Nogi, Surf. Coat. Technol. 98 (1998) 1008.
[3] O. Banakh, P.E. Schmid, R. Sanjines, Surf. Coat. Technol. 163/164 (2003) 57.
[4] A.E. Reiter, V.H. Derflinger, B. Hanselmann, Surf. Coat. Technol. 200 (2005) 2114.
[5] J. Romero, M.A. Gomez, J. Esteve, Thin Solid Films 515 (2006) 113.
[6] R. Franz, J. Neidhardt, B. Sartory, Tribol. Lett. 23 (2006) 101.
[7] J.L. Endrino, G.S. Fox-Rabinovich, C. Gey, Surf. Coat. Technol. 200 (2006) 6840.
[8] Y. Makino, Surf. Coat. Technol. 193 (2005) 185.
[9] A. Sugishima, H. Kajioka, Y. Makino, Surf. Coat. Technol. 97 (1997) 590.
[10] H. Willmann, P.H. Mayrhofer, P.O.A. Persson, Scr. Mater. 54 (2006) 1847.
[11] K. Bobzin, E. Lugscheider, R. Nichel, Mater.wiss. Werkst.tech. 37 (2006) 833.
[12] A. Madan, I.W. Kim, S.C. Cheng, Phys. Rev. Lett. 78 (1997) 1743.
[13] G.Y. Li, J.J. Lao, J.W. Tian, J. Appl. Phys. 95 (2004) 92.
[14] I.W. Kim, Q. Li, L.D. Marks, Appl. Phys. Lett. 78 (2001) 892.
[15] P.E. Van Camp, V.E. Van Doren, J. Devreese, Phys. Rev., B 44 (1991) 9056.
[16] M. Ueno, A. Onodera, Phys. Rev., B 45 (1992) 10123.
[17] P. Ravindra, S. Amin, S. Max, J. Mater. Res. 8 (1993) 1922.
[18] I. Grczyca, N.E. Christensen, P. Perlin, I. Grzegory, Solid State Commun. 79 (1991) 1033.
[19] M. Setoyama, A. Nakayama, M. Tanaka, Surf. Coat. Technol. 86–87 (1996) 225.
[20] K. Bobzin, E. Lugscheider, M. Maes, Surf. Coat. Technol. 200 (2005) 1560.
[21] M. Brizuela, A. Garcia-Luis, I. Braceras, Surf. Coat. Technol. 200 (2005) 192.
[22] E. Spain, J.C. Avelar-Batista, M. Letch, Surf. Coat. Technol. 200 (2005) 1507.
[23] R.A. Young, The Rietveld Method, Oxford University Press, Oxford, UK, 1993, p. 1.
[24] A. Perry, Thin Solid Films 107 (1983) 167.
[25] J. Valli, J. Vac. Sci. Technol., A, Vac. Surf. Films 3 (1985) 2411.
[26] D.N. Lee, J. Mater. Sci. 24 (1989) 4375.
[27] P.V. Essen, R. Hoy, J.D. Kamming, Surf. Coat. Technol. 200 (2006) 3496.
[28] R. Pandey, A. Sutjianto, M. Seel, J. Mater. Res. 8 (1993) 1922.
[29] M. Ueno, A. Onodera, O. Shimomura, Phys. Rev., B 45 (1992) 10123.
[30] N.E. Christensen, I. Gorczyce, Phys. Rev., B 478 (1993) 4307.
[31] R. Wuhrer, W.Y. Yeung, Scr. Mater. 50 (2004) 1461.
[32] E. Lugscheider, K. Bobzin, T. Homig, M. Mase, Thin Solid Films 420–421 (2002) 318.
[33] D.J. Dyson, X-ray and Electron Diffraction Studies in Materials Science, Maney publishing, 1 Carlton House Terrace, London, 2004.
[34] D.R. McKenzie, D.J.H. Cockayne, D.A. Muller, J. Appl. Phys. 70 (1991) 3007.
[35] M. Chhowalla, H.E. Unalan, Nat. Mater. 4 (2005) 317.
[36] A.J. Perry, J. Vac. Sci. Technol., A, Vac. Surf. Films 8 (1990) 1351.
[37] A.G. Evans, J.W. Hutchinson, Int. J. Solids Struct. 20 (1984) 455.